PCCP

RSC Publishing

PAPER

View Article Online
View Journal | View Issue

Cite this: *Phys. Chem. Chem. Phys.*, 2013, **15**, 2847

Low-cost industrially available molybdenum boride and carbide as "platinum-like" catalysts for the hydrogen evolution reaction in biphasic liquid systems†

Micheál D. Scanlon,[a] Xiaojun Bian,[b] Heron Vrubel,[c] Véronique Amstutz,[a] Kurt Schenk,[d] Xile Hu,[c] BaoHong Liu[b] and Hubert H. Girault*[a]

Received 14th December 2012,
Accepted 18th December 2012

DOI: 10.1039/c2cp44522k

www.rsc.org/pccp

Rarely reported low-cost molybdenum boride and carbide microparticles, both of which are available in abundant quantities due to their widespread use in industry, adsorb at aqueous acid–1,2-dichloroethane interfaces and efficiently catalyse the hydrogen evolution reaction in the presence of the organic electron donor – decamethylferrocene. Kinetic studies monitoring biphasic reactions by UV/vis spectroscopy, and further evidence provided by gas chromatography, highlight (a) their superior rates of catalysis relative to other industrially significant transition metal carbides and silicides, as well as a main group refractory compound, and (b) their highly comparable rates of catalysis to Pt microparticles of similar dimensions. Insight into the catalytic processes occurring for each adsorbed microparticle was obtained by voltammetry at the liquid–liquid interface.

1. Introduction

The development of a hydrogen economy to transition from the current fossil fuel based one is a grand challenge requiring the resolution of a myriad of complex scientific, technological and infrastructural matters.[1–4] In this article we address the issue of sustainably producing H_2. The production of H_2 requires an input of energy and proton-rich starting compounds, ideally water. The *i*nterface between *t*wo *i*mmiscible *e*lectrolyte *s*olutions (ITIES)[5–9] represents a suitable methodology to probe biphasic proton coupled electron transfer (PCET) reactions involving aqueous protons and organic soluble molecular electron donors.[10–14] This methodology has also been applied to the study of amphiphilic porphyrins and phthalocyanines as oxygen reduction reaction (ORR) molecular electrocatalysts.[15–23]

Biphasic systems offer a new perspective for the production of hydrogen. The reduction of protons at defect free soft electrified water–1,2-dichloroethane interfaces has been studied intensely since 2008.[10–13] The interfacial Galvani potential difference may be controlled potentiostatically or chemically (by distribution of electrolyte ions) and used to pump protons from the aqueous to the oil phase.[11] Under anaerobic conditions this enables their reduction to H_2 in the presence of organic reducing agents such as cobaltocene[24] and decamethylferrocene (DMFc)[11,13] in the dark and decamethylosmocene[25] and osmocene[26] under UV/vis irradiation. A key focus of our research has been to catalyse the hydrogen evolution reaction (HER) at the ITIES. Previously, we have catalysed the reaction with DMFc by the *in situ* reduction of metallic salts, forming adsorbed metallic nanoparticles (NPs) of Pt or Pd.[27] The use of noble Pt and Pd NPs as highly efficient hydrogen evolution catalysts (HECs), while an excellent proof of concept experiment, has reduced large-scale applicability due to the high prices, limited availability and growing demand for these elements.[28,29] This inspired investigations into the use of the rigorously characterised (by both experimental and computational means) non-noble, more earth abundant nanocrystalline MoS_2 as an adsorbed HEC at the ITIES.[30] A follow-up study maximising the number of catalytic edge sites per mole of MoS_2, by either exfoliating the catalyst or generating NPs on conductive carbon supports, optimised the catalytic activity.[31]

Herein, we report that molybdenum carbide (Mo_2C) and boride (MoB) are highly active biphasic HECs. Key attributes of Mo_2C and MoB that set them apart as HEC candidates are their

[a] *Laboratoire d'Electrochimie Physique et Analytique (LEPA), Ecole Polytechnique Fédérale de Lausanne (EPFL), Station 6, CH-1015 Lausanne, Switzerland. E-mail: Hubert.Girault@epfl.ch; Fax: +41 21 693 3667; Tel: +41 21 693 3145*
[b] *Department of Chemistry, Institute of Biomedical Sciences, Fudan University, Shanghai, 200433, P.R. China*
[c] *Laboratory of Inorganic Synthesis and Catalysis (LSIC), EPFL, BCH-3305, CH-1015 Lausanne, Switzerland*
[d] *Institut des Sciences et Ingénierie Chimiques (ISIC) and Institut de Physique des Systèmes Biologiques (IPSB), EPFL, CH-1015, Lausanne, Switzerland*

† Electronic supplementary information (ESI) available: Calculated equilibrium concentrations and $\Delta_o^w\phi$ for biphasic experiments, optimisation of the quantity of catalyst for kinetic analysis, determination of the reaction order with respect to protons, control cyclic voltammetry experiments, and derivation of the Nernst equation for the biphasic HER. See DOI: 10.1039/c2cp44522k

stability, availability and low-cost due to their widespread use in industry. Mo_2C is stable under both acidic and basic conditions[32] (a rare trait for HECs, particularly with regard to efficient water splitting under acidic conditions), while MoB is stable under acidic but prone to degradation under basic conditions.[32] In comparison to MoS_2, there is a dearth of research on these transition metal carbides and borides as HECs. Recently, two of us highlighted for the first time that MoB is an active HEC.[32] To our knowledge, Mo_2C has only been explicitly reported as a stand-alone active HEC in the aforementioned paper[32] and additionally in a recent article by Schröder's group where they undertook a systematic study of 18 different IV B–VI B transition metal carbides, nitrides, sulphides, silicides and borides, as well as 3 main group refractory compounds as electrocatalytic HECs in acidic electrolyte solutions.[33] Prior to these reports Mo_2C served as a stable, low-cost support for monolayer amounts of precious metals such as Pt and Pd, thereby decreasing the cost of H_2 production from water splitting.[34] Also, Chen and co-workers investigated the stability thresholds of Mo_2C and the more widely studied tungsten carbides (W_2C and WC) as electrocatalysts over different ranges of pH and potential values.[35,36]

Tungsten carbides have been extensively studied as HECs since the 1970s when Levy and Boudart noted that they catalysed several reactions previously only catalysed by Pt.[37] The unexpected catalytic activity has been attributed to their "Pt-like" electronic structures arising from the modification of the nature of the transition metal d-band on carbide formation.[38] Furthermore, tungsten carbides are more resistant to carbon monoxide[39] and sulphur[40] poisoning than Pt.

In this article we highlight Mo_2C and MoB's superior biphasic HER catalytic activities by carrying out a comparative kinetic study with other transition metal carbides (tungsten carbides; W_2C and WC) and silicides (molybdenum silicide; $MoSi_2$), as well as a refractory main group compound (boron carbide; B_4C) and Pt microparticles. Importantly, each of the elements that constitute the non-noble materials considered above are orders of magnitude more abundant[41] and less expensive[34,42,43] than Pt-group metals (Ru, Rh, Pd, Ir, and Pt). Mo_2C, MoB, W_2C, WC, and B_4C play key roles in industrial machinery as cutting tools and abrasives due to their high melting temperatures, hardness, oxidation resistance and excellent chemical stability.[44–46] B_4C is even used as a neutron radiation adsorbent in nuclear applications[47] and $MoSi_2$ has received considerable attention with regard to high-temperature applications.[48] Thus, these materials may be realistically used in large scale HER applications immediately, in contrast to catalysts requiring specialised laboratory preparations.

2. Experimental

Chemicals

All chemicals were used as received without further purification, with the exception of decamethylferrocene (DMFc, ≥99%, Alfa Aesar) which was purified by vacuum sublimation at 140 °C before use.[49] All aqueous solutions were prepared with ultra pure water (Millipore Milli-Q, specific resistivity 18.2 MΩ cm). The solvents used were 1,2-dichloroethane (1,2-DCE, ≥99.8%, Fluka), hydrochloric acid (HCl, 37%, Merck), and sulphuric acid (H_2SO_4, 98%, Merck). Lithium tetrakis(pentafluorophenyl)borate diethyletherate (LiTB-DEE, Boulder Scientific) and bis(triphenylphosphoranylidene) ammonium chloride (BACl, 97%, Aldrich) were used to prepare bis(triphenylphosphoranylidene) ammonium tetrakis(pentafluorophenyl)borate (BATB) by metathesis of equimolar solutions of BACl and LiTB-DEE in a methanol–water (2 : 1 v/v) mixture. The resulting precipitates were filtered, washed and recrystallised from acetone.[50] Molybdenum carbide and boride (Mo_2C and MoB, ~325 mesh, ≥99.5%), molybdenum silicide ($MoSi_2$, ≥99%), boron carbide (B_4C, ~200 mesh, 98%) and platinum powder (0.15–0.45 μm, 99.9%) were purchased from Aldrich. Tungsten carbides (WC and W_2C, ≥99%) were provided by Alfa Aesar. Each of these carbides, borides and silicides were stored under a nitrogen atmosphere until use. Lithium chloride anhydrous (LiCl, ≥99%) and tetraethylammonium chloride (TEACl, ≥98%) were ordered from Fluka.

Particle characterisation

The morphologies and sizes of the particles investigated as potential HECs were investigated by scanning electron microscopy (SEM) secondary electron images obtained using a Phillips (FEI) XLF-30 FEG Schottky field-emission scanning electron microscope operated at beam voltages between 1 and 30 keV. Beam voltages were adjusted to minimise charging effects.

Crystal structures were characterised by X-ray powder diffraction (XRD) diagrams, recorded on an X'Pert MPD PRO from PANalytical equipped with a secondary graphite (002) monochromator and an X'Celerator detector operated in Bragg–Brentano geometry. The samples were lightly ground and fixed to a rotating Si monocrystal by means of vaseline. A step size of 0.008° was chosen and an acquisition time of 2 min per degree.

ICP-OES analysis was performed using an Optima 2000 spectrometer (Perkin-Elmer). Molybdenum, boron and tungsten contents were determined using the intensity of the following emission lines: Mo – 203.845 nm; B – 208.957 nm; W – 207.912 nm. Standards TraceCERT were purchased from Aldrich and used for calibration. A known amount, between 2 and 5 mg, of the sample to be analysed was weighed in a vial. For MoB and Mo_2C, 1 mL of *aqua regia* was added to the vials and heated to 80 °C to give a homogeneous solution. The solution was quantitatively transferred to a 100 mL volumetric flask using a 5% nitric acid solution. For W_2C and WC, the solids were weighed in a tall shape vial and 3 mL of *aqua regia* was added. The vials were directly heated on the top of a heating plate set to 120 °C. To the hot solutions, 2 mL of 30% H_2O_2 was added dropwise until a colourless solution was obtained. The colourless solution quickly converts to a yellow suspension of WO_3. After cooling, the yellow solid was carefully dissolved by adding 3 M KOH solution to convert the WO_3 to the soluble WO_4^{2-}. The final solution was transferred to a 100 mL volumetric flask using pure deionised water. The ICP emission of these samples was collected immediately after the preparation of the solutions.

Zeta (ζ)-potential measurements were carried out on a Nano ZS Zetasizer (Malvern Instruments, U.K.), with irradiation (λ = 633 nm) from a He–Ne laser, using Dispersion Technology Software (DTS). Each particle suspension (1 mg/5 ml) was initially dispersed in an aqueous NaOH solution, pH 12, and sonicated for at least 15 minutes to ensure a uniform dispersion free of any agglomerated particles. The pH was subsequently adjusted incrementally, while stirring, to approximately pH 2 by dropwise addition of 0.5 M HCl and monitored using a Metrohm 632 pH meter. Samples (approximately 0.75 mL) were injected at regular pH intervals into a folded capillary cell. The ζ-potential (mV) was elucidated from the measured electrophoretic mobility using the Smoluchowski approximation[51,52] of Henry's equation.[52,53]

Shake flask experiments

All shake flask experiments, whether analysed by gas chromatography or UV/vis spectroscopy, were completed using aqueous and organic solutions thoroughly de-gassed with nitrogen, under anaerobic conditions in a glove box purged with nitrogen, in the dark, and at an ambient temperature of 23 ± 2 °C. Anaerobic conditions were necessary to avoid competing side-reactions with oxygen, such as H_2O_2 generation.[10,13,15,18,20,22]

Analysis of $H_{2(g)}$ evolved. Two-phase reactions were performed in a septum sealed glass vial (pictured in Scheme 1). 2 mL of an acidic aqueous phase containing LiTB-DEE, with or without a catalyst, was contacted with an equal volume of 1,2-DCE containing the lipophilic electron donor DMFc. Magnetic stirring (900 rpm) was used to emulsify the two phases for the duration of each experiment (1 h). None of the microparticles investigated herein were soluble in the organic or aqueous phases, as seen previously for MoS_2[30] and its various carbon-supported forms.[31] If the two mechanically emulsified phases were allowed to settle the microparticles would sediment at the liquid–liquid interface. This preferential adsorption at the interface, driven by the minimisation of the interfacial free energy in the system, occurs when the interfacial tension of the two immiscible fluids is higher than the difference of the interfacial tension of the microparticle-aqueous phase and microparticle-organic phase, respectively.[54,55] The liquid–liquid interface was polarised chemically by distribution of a common ion (highly hydrophobic TB^-, initially present in the aqueous phase) across the interface. The precise composition of the shake flask is illustrated in Scheme 1. 1 mL samples of the headspace gas were obtained using a lock-in syringe with a push–pull valve (SGE Analytical Sciences) in the glovebox and subsequently analysed by gas chromatography (GC) using a Perkin-Elmer GC (Clarus 400, equipped with 5 Å molecular sieves and an 80/100 mesh) with a thermal conductivity detector (TCD) and argon as the carrier gas.

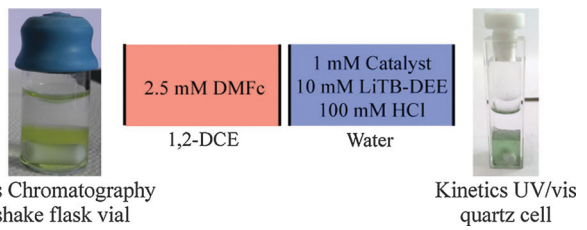

Scheme 1 Biphasic hydrogen evolution under chemical polarisation: schematic representation of the initial compositions of the aqueous and organic phases. The products of the biphasic reactions, hydrogen gas and organic solubilised $DMFc^+$ were monitored by gas chromatography and UV/vis spectroscopy, respectively.

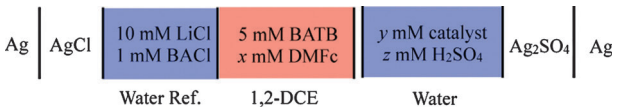

Scheme 2 Schematic representation of the compositions of the electrochemical cell used for ion transfer voltammetry.

Kinetic studies. The composition of the shake-flask used for kinetic studies was identical to that analysed by gas chromatography (see Scheme 1). UV/vis spectra of the product of the biphasic reaction, decamethylferrocenium cations ($DMFc^+$), were measured on an Ocean Optics CHEM2000 spectrophotometer using a quartz cuvette with a path length of 10 mm, volume of 4 mL, and equipped with a teflon cap to prevent evaporation of the organic phase during analysis (the quartz cuvette is pictured in Scheme 1, 1 mL of each phase was added to the cell). UV/vis scans were taken at regular intervals over a period of 30 mins. During scan intervals the solution in the cuvette was constantly agitated using a magnetic stirrer (900 rpm). A molar extinction coefficient (ε) of $DMFc^+$ in 1,2-DCE was determined previously to be 0.632 mM^{-1} cm^{-1}.[30]

Electrochemical measurements at the liquid–liquid interface

Ion-transfer voltammetry experiments at the water–1,2-DCE interface were performed in a four-electrode configuration using a PGSTAT 30 potentiostat (Metrohm, CH). Two platinum counter electrodes were positioned in the aqueous and organic phases, respectively, to supply the current flow. An external potential was applied by means of silver/silver sulphate ($Ag/AgSO_4$) and silver/silver chloride (Ag/AgCl) reference electrodes, which were connected to the aqueous and 1,2-DCE phases, respectively, *via* a Luggin capillary as illustrated previously.[30] The Galvani potential difference across the interface ($\Delta_o^w\phi$) was estimated by taking the formal ion transfer potential of tetraethylammonium cations (TEA^+) as 0.019 V.[56] The obtained voltammetry was not *iR* compensated. The area of the liquid–liquid interface was 1.53 cm^2. The generic composition of the four-electrode cells studied is illustrated in Scheme 2. As per the shake-flask experiments, sedimentation of the microparticles was observed at the interface, in particular at the oil–water–glass three-phase junction, driven by minimisation of the systems' interfacial free energy. All voltammetry experiments were completed using aqueous and organic solutions thoroughly de-gassed with nitrogen, under anaerobic conditions in a nitrogen filled glove box and at an ambient temperature of 23 ± 2 °C.

3. Results and discussion

Particle characterisation

All particles chosen for study (Mo_2C, MoB, W_2C, WC, $MoSi_2$ and B_4C) were purchased from commercial sources and their

compositions confirmed by ICP-OES analysis. Comparisons of the experimentally found elemental percentages perfectly matched those theoretically calculated (in brackets), *i.e.* for Mo_2C: Mo – 93.8% (94.1%); for MoB: Mo – 90.1% (89.9%); B – 10.0% (10.1%); for WC: W – 93.5% (93.9%) and for W_2C: W – 96.7% (96.8%). The extreme thermal and chemical stabilities of $MoSi_2$ and B_4C prevented their analysis by ICP-OES.

SEM images reveal that Mo_2C, MoB and W_2C have particle sizes in the range of 1–3 μm (Fig. 1). WC consists of smaller 0.5–1 μm sized particles present as large *ca.* 10 μm agglomerates. B_4C and $MoSi_2$ consist of larger particles, with sizes ranging from 4–10 and 4–12 μm, respectively. The large $MoSi_2$ particles were decorated with smaller 1–2 μm sized particles. The morphologies of B_4C and $MoSi_2$ were more crystalline in nature than the more rounded, sintered shapes of the individual particles of Mo_2C, MoB, W_2C and WC.

XRD was used to verify the bulk crystal structures of as-received W_2C, WC, B_4C, and $MoSi_2$ (Fig. 2). The XRD patterns were found to be consistent with hexagonal WC (space group $P\bar{6}m2$, ICDD-Number 04-004-7120), trigonal W_2C (space group $P\bar{3}m1$, ICDD-Number 04-008-1623), tetragonal $MoSi_2$ (space group $I4/mmm$) and trigonal B_4C (space group $R3m$) by comparison of the experimentally obtained XRD patterns with those computed from phases obtained from X'Pert HighScore, Version 2.2.5 (2009, PANalytical B.V., Almelo, The Netherlands). Phase purity was observed for $MoSi_2$. Each of the other particles contained some phase impurities. In the sample with predominantly W_2C, the weight percentages found by a Rietveld refinement using HighScore were W_2C : WC = 89.90 (±0.03) : 10.10 (±0.01), while in the sample with predominantly WC, the weight percentages were W_2C : WC = 3.14 (±0.08) : 96.90 (±0.02). Additional XRD peaks in the B_4C pattern at 13°, 21° and 25° may be attributed to impurities arising from some allotropic form of carbon. Also, the broad hump in the pattern below 25° is indicative of amorphous carbon. The presence of such carbon impurities is unsurprising since B_4C is in equilibrium with free carbon and the synthesis of B_4C without the presence of free carbon is known to be quite challenging.[57,58] Previously, two of us have obtained the XRD patterns for Mo_2C and MoB. Using an identical analysis it was found that the Mo_2C particles were exclusively in the hexagonal form (space group $P6_3/mmc$) while the MoB particles were mainly in the tetragonal form (space group $I4_1/amd$), with some minor phase impurities present.[32]

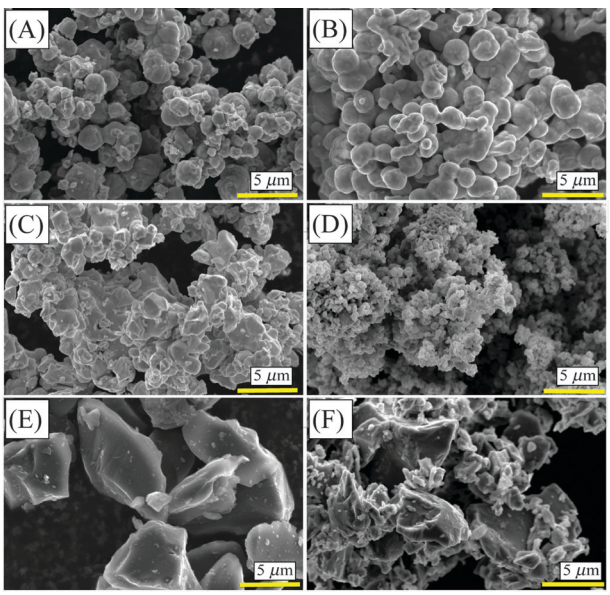

Fig. 1 Scanning electron microscopy (SEM) images of commercial (A) Mo_2C, (B) MoB, (C) W_2C, (D) WC, (E) B_4C and (F) $MoSi_2$ particles, magnification 10.0 k.

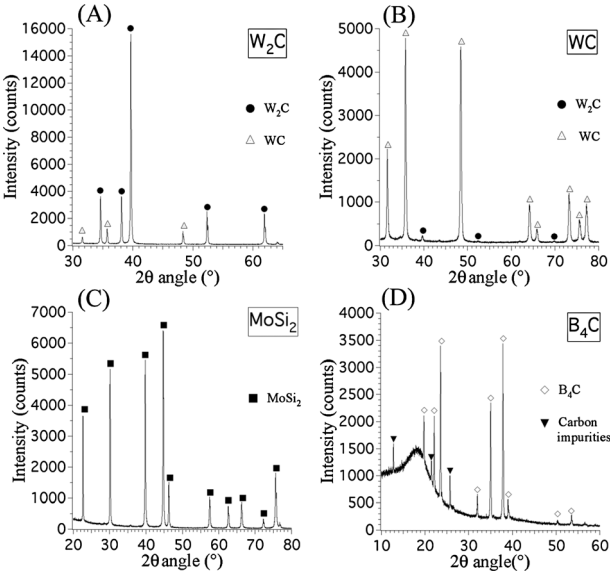

Fig. 2 X-ray diffraction (XRD) patterns of (A) W_2C, (B) WC, (C) $MoSi_2$ and (D) B_4C.

Zeta (ζ)-potential measurements of each microparticle reveal that over the entire pH range accessible to analysis using the zetasizer, approximately between pH 2 and 11, each particle exhibits a negative surface charge (Fig. 3). Such negative ζ-potentials indicate that the surfaces of each particle are covered in strongly acidic surface oxide species. Surface oxides have been reported to form on Mo_2C,[32,35,36,59–61] MoB,[32] W_2C or WC,[35,36,62,63] B_4C[64] and $MoSi_2$[65] even at ambient temperatures and pressures. Most oxide surfaces are hydrated and, thus, dominated by hydroxyl groups. These surface groups are amphoteric and can result in a negative or a positive surface charge according to[62]

$$\equiv M\text{–}OH \leftrightarrow \equiv M\text{–}O^- + H^+ \quad (1)$$

$$\equiv M\text{–}OH + H^+ \leftrightarrow \equiv M\text{–}OH_2^+ \quad (2)$$

where M is the metal of the oxide species. The surface dissociation reactions are dependent on pH meaning that the oxide will either be acidic or basic depending on its dissociation constant. Thus, for acidic oxides the surface hydroxyl groups will dissociate even at low pH resulting in negative surface charges, *e.g.* MoO_4^{2-}, WO_4^{2-}, *etc.*, as observed in Fig. 3. Indeed, an activation period for the HER under acidic conditions has been reported for Mo_2C and MoB catalysts embedded in soft carbon-paste

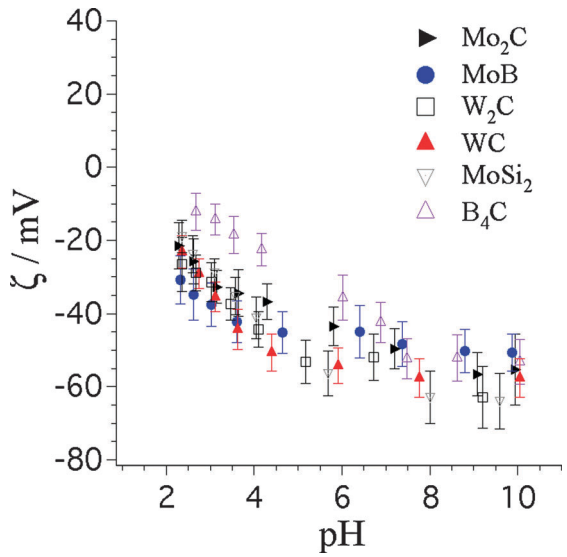

Fig. 3 Zeta (ζ)-potential measurements (mV) of each catalytic microparticle as a function of pH in aqueous dispersions at a concentration of 1 mg/5 ml. The error bars in the *y*-direction represent the standard deviation of the ζ distribution around the mean result.

electrodes and directly attributed to the time required to rid their surfaces of these poorly catalytic surface oxides during constant current electrolysis.[32]

Biphasic HER monitored by gas chromatography: initial screening of potential catalysts

The relative activities of each precious and nonprecious material (Pt, Mo_2C, MoB, W_2C, WC, $MoSi_2$ and B_4C) as hydrogen evolution catalysts (HECs) were initially investigated by biphasic "shake-flask" reactions with chemically controlled polarisation of the interface.[10,66] As outlined in Scheme 1, an aqueous solution (w) containing 100 mM HCl, 10 mM LiTB-DEE and 1 mM catalyst was contacted with a 1,2-DCE solution containing 2.5 mM DMFc under anaerobic conditions with stirring. The role of the TB^- anion is to act as a phase transfer catalyst for the extraction of protons to the organic phase (o) as hydrogen tetrakis(pentafluorophenyl)borate diethyletherate (HDEETB, hereafter referred to as HTB for simplicity, see eqn (3)). Diethyletherate acts as a lipophilic base.

$$H^{+,w} + TB^{-,w} \rightarrow HTB^{o} \quad (3)$$

Taking into account the Nernst equation for the distribution of all common ions, the mass balance of all ions in both phases and the electroneutrality conditions for both phases, the following equation may be arrived at (as derived in the supporting information of several recent publications)[20,22,67]

$$\sum_i z_i F c_i^{w} = \sum_i \frac{z_i F c_{i,\text{total}}}{1 + \frac{V^{o}}{V^{w}} \exp\left[\frac{z_i F}{RT}\left(\Delta_o^w\phi - \Delta_o^w\phi_i^0\right)\right]} \quad (4)$$

where $\Delta_o^w\phi_i^0$ is the formal ion transfer potential of species i, V^w and V^o are the water and oil phase volumes, respectively, $c_{i,\text{total}}$ and c_i^w are the initial total concentration of i present prior to equilibrium and the concentration of i in the aqueous phase at equilibrium, respectively, and all other terms have their usual meanings. Using eqn (4), the initial partition of the individual electrolyte ions in the biphasic system outlined in Scheme 1 established an interfacial Galvani distribution potential ($\Delta_o^w\phi$) of 0.523 V for all common ions at equilibrium. The calculation was performed using Mathematica Software (version 7.0). This potential was sufficient to extract protons in the form of HTB (thus, fulfilling the electroneutrality conditions) to 1,2-DCE almost quantitatively with a concentration of 9.89 mM at equilibrium (Table S1, ESI†). The transferred protons may undergo reduction by the electron donor, DMFc, in the organic phase until the supply of DMFc is exhausted (eqn (5)).[12,31]

$$DMFc^{o} + H^{+,o} \xrightarrow{\text{catalyst in 1,2-DCE}} DMFc^{+,o} + \frac{1}{2}H_2 \quad (5)$$

However, as this biphasic reaction is carried out under stirring conditions, it is not possible to unequivocally state the locus of the reaction and discern a strictly heterogeneous reaction from a homogeneous one. Alternatively, an interfacial reaction upon polarisation of the interface may take place between organic solubilised DMFc and aqueous protons (eqn (6)).[12,31]

$$DMFc^{o} + H^{+,w} \xrightarrow{\text{interfacial catalyst}} DMFc^{+,o} + \frac{1}{2}H_2 \quad (6)$$

Another possibility is that since DMFc is sparingly soluble in the aqueous phase, one must at least consider that electron transfer may take place in the aqueous phase as outlined in eqn (7) and (8).[12,30]

$$DMFc^{o} \rightarrow DMFc^{w} \quad (7)$$

$$DMFc^{w} + H^{+,w} + TB^{-,w} \xrightarrow{\text{catalyst in aqueous phase}} DMFc^{+,o} + TB^{-,o} + \frac{1}{2}H_2 \quad (8)$$

Irrespective of whether the mechanism proceeds *via* eqn (5), (6) or (8) (or, indeed, if processes take place simultaneously), the driving force for the reaction is the same, as shown previously,[30] and the net result is the complete conversion of DMFc to $DMFc^+$ and the consumption of protons resulting in the evolution of hydrogen gas (H_2). Globally, the reaction is therefore written as

$$DMFc^{o} + H^{+,w} \xrightarrow{\text{catalyst}} DMFc^{+,o} + \frac{1}{2}H_2 \quad (9)$$

The partition of $DMFc^+$ between the phases and the loss of protons will affect $\Delta_o^w\phi$, which is re-calculated to be 0.516 V at a time of full conversion of DMFc to $DMFc^+$, the concomitant consumption of protons and the associated re-distribution of the concentrations of each electrolyte ion at equilibrium have taken place. This value of $\Delta_o^w\phi$ is sufficiently positive to retain $DMFc^+$ ($\Delta_o^w\phi_{tr,j}^0 = -0.26$ V, see Table S1, ESI†) in the organic phase, a crucial point as the concentration of organic solubilised $DMFc^+$ will be probed later as a quantitative measure of the progress of the biphasic HER with time in the absence or presence of various catalysts.

As a simple initial method of screening the HER activity of each potential catalyst the quantities of H_2 gas evolved after 1 h from shake-flask experiments, differing only in the nature of the microparticles initially introduced into the aqueous phase (Scheme 1), were monitored by gas chromatography. Subsequently, comparisons were made to a shake-flask devoid of catalysts carried out under otherwise identical experimental conditions (Fig. 4). The biphasic formation of H_2 is a kinetically slow process as highlighted by the evolution of a mere 0.052 μmol H_2 after 1 h in the absence of a catalyst. This represented 2.08% of the maximum theoretical stoichiometric amount of H_2 that may be evolved (2.5 μmol), see eqn (5) to (9), as limited by the initial quantity of DMFc dissolved in the organic phase (5 μmol). In comparison, and as expected, Pt microparticles increase the reaction rate considerably (1.895 μmol H_2 evolved). Encouragingly, Mo_2C, MoB, W_2C and WC microparticles were also clearly active HECs with 2.22, 1.45, 1.20 and 0.86 μmol H_2 evolved, respectively, and under these experimental conditions Mo_2C outperformed Pt microparticles of similar dimensions. However, $MoSi_2$ and B_4C proved to be poor biphasic HECs with a very minor improvement in the rate observed for $MoSi_2$ (0.145 μmol H_2 evolved) and a deterioration in the rate noted for B_4C (0.039 μmol H_2 evolved) compared to that seen in the absence of a catalyst. Taking these observations into account, B_4C did not warrant a further in-depth study and was eliminated as a potential HEC. B_4C's inactivity may be attributed to a lack of electrocatalytic d-electrons, reported to play a crucial role in the "Pt-like" electronic structures adopted by transition metal carbides and borides,[33,44] discussed later.

Biphasic HER monitored by UV/vis spectroscopy: kinetic studies

The kinetically limited progress of the biphasic HER in the presence or absence of catalytic microparticles can be accurately assessed by monitoring changes in the UV/vis adsorption spectra for the conversion of organic solubilised DMFc (λ_{max} = 425 nm) to $DMFc^+$ (λ_{max} = 779 nm) with time (see Scheme 1).[30,31] A preliminary experiment was carried out using Mo_2C and MoB microparticles (catalytically the most efficient nonprecious materials) to optimise the quantity of a catalyst required to achieve a maximal rate. The quantity of a catalyst introduced into the aqueous phase was varied from 0.25 to 2.5 mM and it was shown that 1 mM of Mo_2C or MoB was sufficient to achieve maximal rates of catalysis, the variation in the rate with catalyst concentration being more pronounced for Mo_2C (Fig. S1, ESI†). The maximum stoichiometric amount of $DMFc^+$ (2.5 mM), limited by the initial DMFc concentration (2.5 mM), was attained for Mo_2C, MoB and Pt microparticles within the experimental time-frame of 1800 s (Fig. 5(A)). However, after 1800 s, slower kinetics for the biphasic HER in the presence of W_2C, WC, $MoSi_2$ and in the absence of a catalyst impeded complete consumption of the electron donor DMFc (Fig. 5(A)). The initial rates of reaction were quickest for Mo_2C, followed by MoB, which was in turn closely followed by Pt. However, as shown later, Pt exhibits different kinetics to Mo_2C and MoB and the exhaustion of DMFc occurred more rapidly in the presence of Pt than MoB. Both tungsten carbides were considerably less active, W_2C being the more active of the two. Finally, $MoSi_2$ produced a barely perceptible increase in the rate compared to the situation in the absence of a catalyst and was also eliminated at this stage as a material of interest for HEC applications.

The reaction order in the presence of each catalyst with respect to [DMFc] was obtained by plotting the logarithm of the reaction rate (estimated from the slope of the polynomial fit to the experimental data) *vs.* the logarithm of [DMFc] (Fig. 6(A), data not shown for W_2C and WC). The rate of reaction with respect to [DMFc] was found to be first order in the presence of Mo_2C and MoB microparticles and zero order in the presence of Pt, W_2C and WC microparticles. Due to the extremely slow rates of reaction obtained both in the absence of a catalyst and in the presence of $MoSi_2$ the polynomial fits to this experimental data were inadequate to irrefutably assign a specific reaction order and consequently no fitting was applied to these data. Subsequently, the reaction order was found to be independent of proton concentration, when $[H^+] > 1$ mM, in the presence of Mo_2C and MoB microparticles, by plotting Ln(v)–Ln([DMFc]) *vs.* Ln([H^+]), and Pt, W_2C, and WC microparticles, by plotting Ln(v) *vs.* Ln([H^+]) (Fig. S2, ESI†). Therefore, the rate of reaction for the biphasic HER catalysed by Mo_2C and MoB microparticles can be written as

$$v = \frac{d[DMFc^{+,o}]}{dt} = k[DMFc^{o}] \quad (10)$$

where k is the apparent rate constant of the reaction. The integrated rate law was simply expressed as[68]

$$kt = \ln\frac{a}{a-x} \quad (11)$$

where a is the initial concentration of DMFc in 1,2-DCE (denoted $[DMFc]_0$) and x is the concentration of $DMFc^+$.

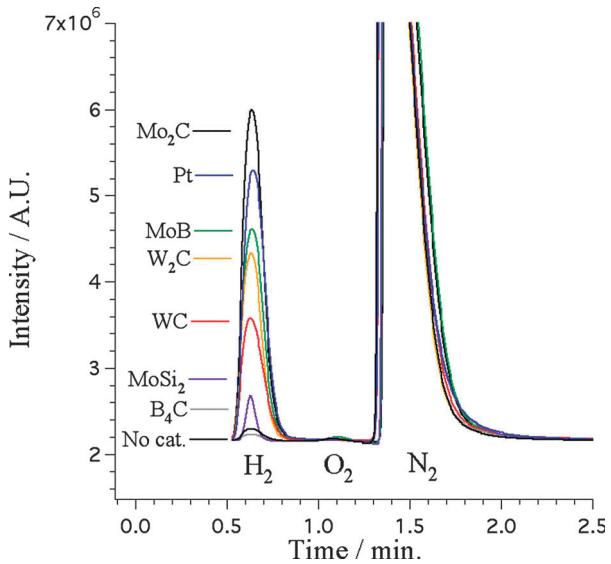

Fig. 4 Gas chromatograms of the shake-flask headspace for two-phase reactions (see Scheme 1) after 1 h, under anaerobic conditions, both in the absence and presence of each catalytic microparticle, as indicated.

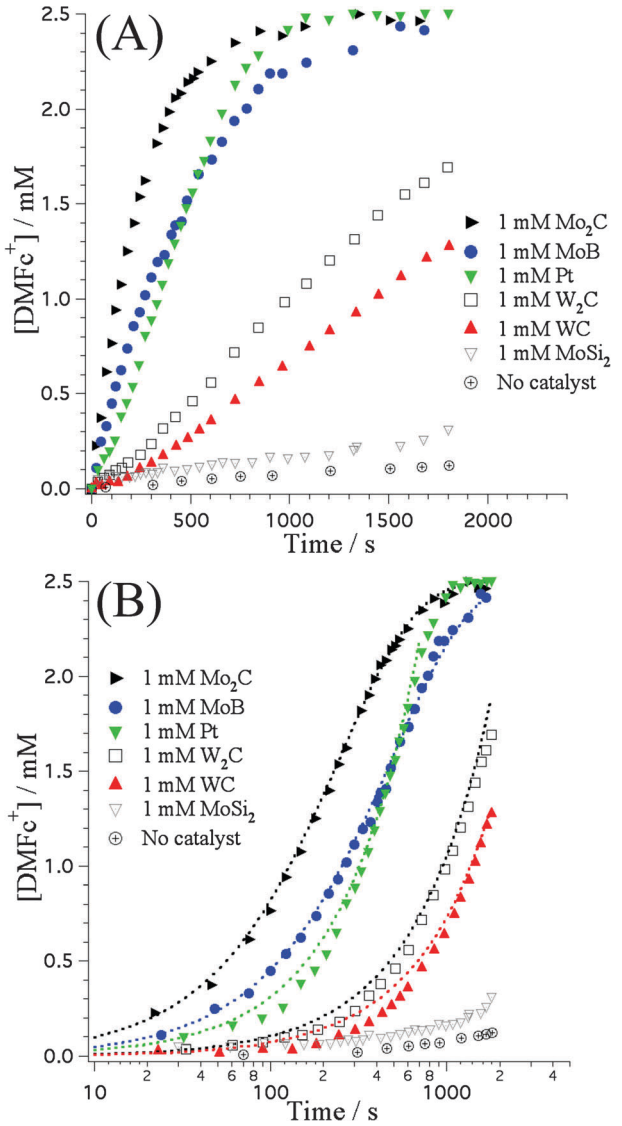

Fig. 5 (A) Kinetics of the biphasic hydrogen evolution reaction (HER) with chemically controlled polarisation, see Scheme 1, in the absence and presence of each catalytic microparticle, as followed by monitoring changes in the UV/Vis absorbance (λ_{max} = 779 nm) for organic solubilised $DMFc^+$. (B) The initial rates of reaction are clarified graphically by using a logarithmic scale for the reaction time. Fits (dotted lines) were obtained from the calculated rate constants (k/mM s^{-1} for zero order kinetics or s^{-1} for first order kinetics, see Table 1).

The rate of reaction catalysed by Pt, W_2C and WC microparticles is constant[68] ($v = k$) and the subsequent rate law expressed as

$$kt = x \text{ for } 0 \leq x \leq a \qquad (12)$$

Plots of the right hand sides of eqn (11) and (12) as a function of time for those catalysts exhibiting first and zero order kinetics with regard to [DMFc], respectively, gave straight lines with slopes of k (Fig. 6(B) and (C)). These calculated rate constants (Table 1), used to determine the theoretical $[DMFc^+]$ in 1,2-DCE as a function of time, reproduced the experimental results (plotted for clarity using a logarithmic scale for the

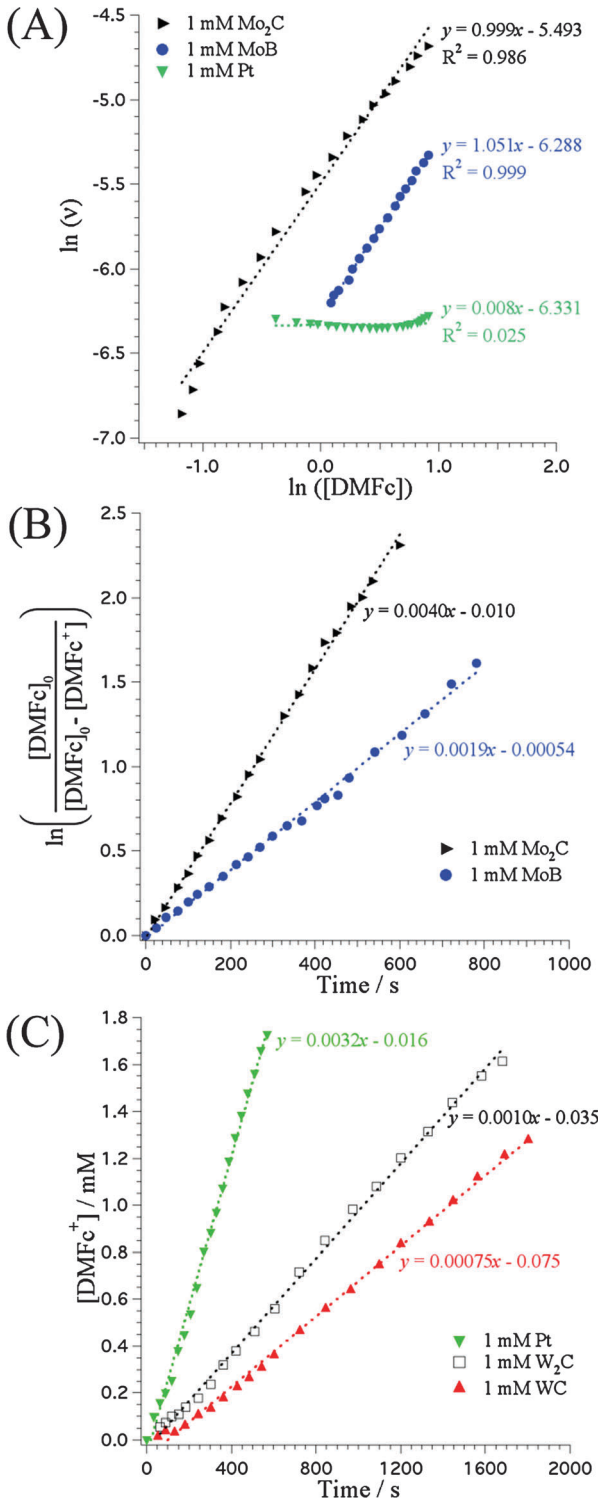

Fig. 6 Rate order determination with respect to DMFc: (A) Ln(v) *vs.* Ln([DMFc]) for the reactions with Mo_2C, MoB and Pt microparticles. The reaction orders were also found to be independent of DMFc concentration for W_2C and WC (data not shown). Determination of rate constants (k): plots of the integrated rate laws, see eqn (11) and (12), *versus* time (s) for the reactions exhibiting overall (B) 1st order kinetics (Mo_2C and MoB) and (C) zero order kinetics (Pt, W_2C, and WC). $[DMFc]_0$ is the initial concentration of DMFc at t = 0 s. The slopes of the straight lines represent the rate constants (k/mM s^{-1} for zero order kinetics or s^{-1} for 1st order kinetics) for each reaction, as tabulated in Table 1. The composition of the biphasic cell used is outlined in Scheme 1.

Table 1 Calculated apparent rate constants (k/mM s^{-1} for zero order kinetics or s^{-1} for 1st order kinetics) for the biphasic reaction in the absence and presence of a catalyst

Catalyst	Order of reaction	k
WC	Zero	0.00075 mM s^{-1}
W_2C	Zero	0.0010 mM s^{-1}
Pt	Zero	0.0032 mM s^{-1}
MoB	1st	0.0019 s^{-1}
Mo_2C	1st	0.0040 s^{-1}

reaction time in Fig. 5(B)) thereby confirming that the assumed rate equations correspond with the experimental data.

If an assumption is made that the reaction in the absence of a catalyst is first order with respect to [DMFc], as has been suggested previously,[30,31] a value of k of 2.3×10^{-5} s^{-1} may be calculated indicating approximate increases of the rate of reaction by factors of 174 and 83 in the presence of Mo_2C and MoB microparticles, respectively. In the literature, the ''Pt-like'' catalytic activity of Mo_2C has been attributed to the permeation of carbon atoms into the lattice of the transition metal, thereby lengthening the metal–metal distance and, thus, increasing the d-band electron density at the Fermi level of molybdenum.[44] The binding energy of an adsorbed species at a catalyst's surface (such as O_2[69] or H_2[70]) and, in effect, the manner of that catalysts' surface interactions with adsorbed atoms or molecules have been shown to depend strongly on the electronic structure of the surface as described by the surface d-band density of states (DOS). Thus, through the work of Nørskov's group in particular,[69–72] a clear link has been established between electronic structure and chemical binding energy, now a key descriptor for the prediction and explanation of catalytic activity. The primary principle is simple: for efficient catalytic activity the reactive intermediate should bond the catalysts surface with a desirable moderate strength, leading to a volcano relationship between catalytic activity and binding energy. However, unlike well-studied MoS_2 where reactive intermediates have been shown to bond with moderate strength at unsaturated edge sites,[71] the surface reactivities of molybdenum boride and carbide are different and as yet relatively unknown. Thus, further spectroscopic, electrochemical, and computational studies are warranted to answer fundamental questions, for example during hydrogen evolution does Mo behave like other metals such as Pt, Ni, and Hg, or are bridging hydride species such as Mo–H–B and Mo–H–C involved?[32]

Voltammetry studies at the liquid–liquid interface

Thus far, the thermodynamic driving force pumping protons into the organic phase and enabling the biphasic HER reaction, see eqn (9), to occur has been provided by chemical distribution of common ions. Further insight into the mechanistic details of these catalysed biphasic reactions may also be gleaned by potentiostatically polarising the interface in a 4-electrode configuration (see Scheme 2 for the electrochemical cell configuration). Fig. 7 shows cyclic voltammograms (CVs) comparing the baseline response of the background electrolytes (no electron donor or catalyst present) with catalytic responses in the presence of organic solubilised DMFc and either Mo_2C, MoB, W_2C, WC, or Pt microparticles (primarily sedimented at the interface). The potential window of the baseline response was limited by reversible proton and SO_4^{2-} transfer, with perhaps some undissociated HSO_4^- transferring also, at the positive and negative potential limits, respectively. In the presence of DMFc and each catalytic microparticle, an irreversible current wave dominates the positive end of the potential window. This irreversible current may be attributed to a proton coupled electron transfer (PCET) event whereby interfacial (see Scheme 3) or organic transferred protons adsorbed on the catalyst's surface undergo rapid electron transfer with DMFc. The resulting heterogeneous evolution of molecular hydrogen fully consumes the protons, according to either eqn (5), (6) or (8), thus explaining the absence of a return peak.

The onset potential of PCET for Pt is *ca.* 100 mV less positive than for each of the transition metal carbides and borides, thus resulting in a higher current density for Pt at the positive limits of the potential window. Previously, the overpotential for the HER at a Pt electrode was also reported to be *ca.* 100 mV less than that for Mo_2C and MoB modified carbon paste electrodes.[32] The early onset of PCET for Pt would suggest that it is a more active catalyst than Mo_2C or MoB, however from the kinetic studies we have clearly shown that this is not necessarily the case for a biphasic system. Interestingly, in the presence of MoB microparticles a small return peak is consistently observed at positive potentials suggesting that perhaps MoB catalyses the biphasic HER *via* a subtly different mechanism to the other microparticles investigated. Also, in comparison to the baseline response, a large interfacial capacitance is observed in the presence of DMFc and each of the catalytic microparticles. Control experiments were performed whereby the catalyst or DMFc (Fig. S3, ESI†) was removed from the electrochemical cell. In both instances no changes in interfacial capacitance were observed compared to the baseline response indicating that all elements in the electrochemical cell, outlined in Scheme 2, must be present to observe the larger than anticipated capacitance. Its specific origin is currently unclear, perhaps an ion-pairing type interaction of electrochemically generated $DMFc^+$ with negatively charged (as shown in Fig. 3) catalytic microparticles, sedimented at the interface, is responsible. Also, in the absence of a catalyst, but in the presence of DMFc, a smaller irreversible current wave at positive potentials is observed and the reverse peak remains due to the incomplete consumption of protons (Fig. S3, ESI†), as reported previously.[30,31]

The Nernst equation for the global biphasic HER (see ESI† for derivation) reads

$$\Delta_o^w\phi_{HER} = \Delta_o^w\phi_{HER}^0 + \frac{RT}{F}\ln\left(\frac{a^o_{DMFc^+}}{a^o_{DMFc}}\right) + \frac{RT}{F}\ln 10\,pH \quad (13)$$

where $\Delta_o^w\phi_{HER}^0 = \left[E^0_{DMFc^+/DMFc}\right]^o_{SHE}/F$ and $\left[E^0_{DMFc^+/DMFc}\right]^o_{SHE}$ signifies the standard redox potential of the $DMFc^+$/DMFc couple in 1,2-DCE with respect to the aqueous standard hydrogen electrode (SHE). $a^o_{DMFc^\beta}$ represents the activity of $DMFc^+$ or DMFc (denoted by β) in 1,2-DCE. Eqn (13) predicts the pH dependence of the redox Galvani potential difference of the hydrogen

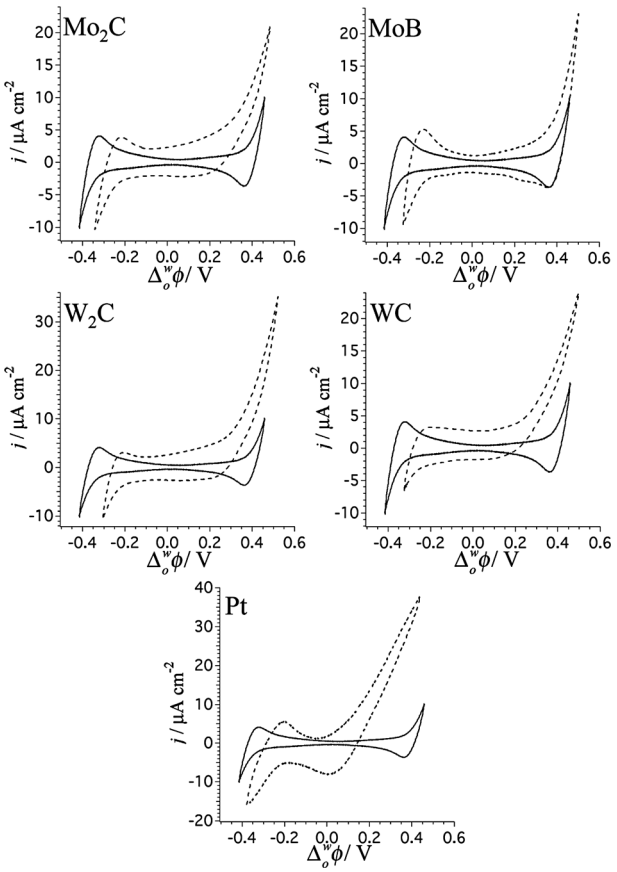

Fig. 7 Influence of the catalyst: cyclic voltammograms for the baseline response ($x = 0$, $y = 0$, solid lines) and the catalytic proton coupled electron transfer (PCET) response in the presence of both DMFc and either Mo_2C, MoB, W_2C, WC, or Pt ($x = 2.5$, $y = 0.5$, dashed lines) at approximately pH 2 ($z = 5$). See Scheme 2 for composition of the electrochemical cell. Scan rates in all cases: 50 mV s^{-1}.

evolution reaction ($\Delta^{w}_{o}\phi^{0}_{HER}$), which was corroborated by the shift of the current signal by about 60 mV pH^{-1} as shown in Fig. 8(A). Additionally, eqn (13) also clearly shows a dependence on the standard redox potential of the organic electron donor. Although not attempted in this study, on substitution of DMFc by a stronger or weaker electron donor, a shift of the onset

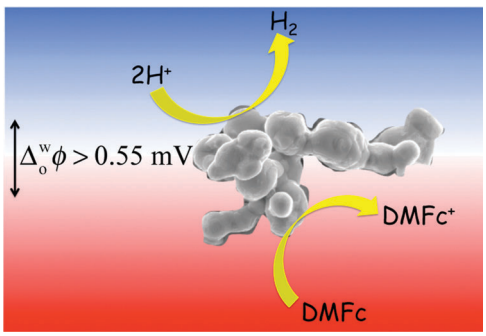

Scheme 3 Schematic of heterogeneous biphasic interfacial proton coupled electron transfer (PCET) with the evolution of molecular hydrogen in the presence of Mo_2C or MoB microparticles at a polarised interface. The aqueous and organic phases are coloured blue and red, respectively.

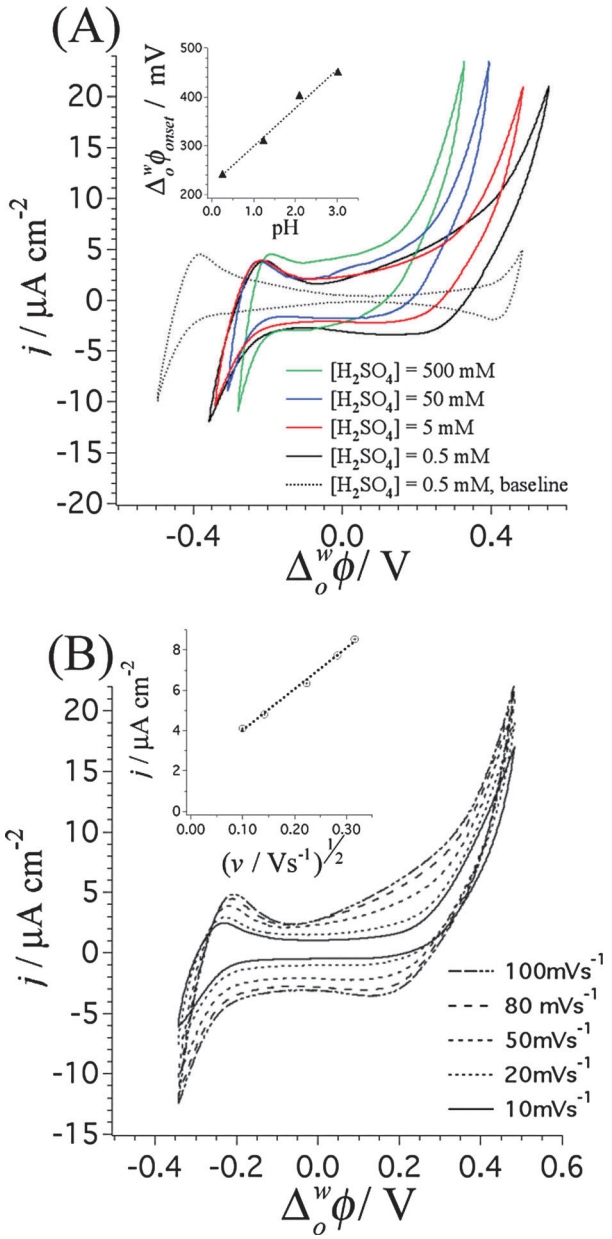

Fig. 8 (A) Influence of pH: cyclic voltammograms for the catalytic proton coupled electron transfer (PCET) response in the presence of both DMFc and Mo_2C ($x = 2.5$, $y = 0.5$, see Scheme 2) for various proton concentrations in the aqueous phase ($z = 0.5$, 5, 50 and 500). Scan rate: 50 mV s^{-1}. Inset: pH dependence of $\Delta^{w}_{o}\phi_{onset}$ at 15 μA cm^{-2} for the PCET response. (B) Scan rate studies: scan rate dependence for the electrochemical cell in the presence of both DMFc and Mo_2C at approximately pH 2 ($x = 2.5$, $y = 0.5$, $z = 5$, see Scheme 2). Inset: plot of current density (j/μA cm^{-2}) *versus* the square root of the scan rate ($(\nu/V\ s^{-1})^{1/2}$) at $\Delta^{w}_{o}\phi = 0.25$ V.

potential for the irreversible current to more negative and positive potentials, respectively, would be expected. Such a trend was previously reported for biphasic reduction of O_2 with ferrocene, ferrocenecarboxaldehyde and 1,1′-dimethylferrocene in the presence of cobalt porphyrin molecular catalysts.[15,19] The long-term electrocatalytic stabilities under strongly acidic conditions of Mo_2C and MoB embedded in soft carbon paste electrodes have been reported.[32] However, the design of such

extended electrolysis experiments at fixed potentials to highlight catalyst stability using biphasic systems is not trivial (for example the electron donor DMFc must be constantly regenerated for many hours and even days). A new biphasic electrolysis cell is currently being developed to test the long-term stability of interfacial catalysts, such as Mo_2C and MoB.

Finally, a scan rate study was performed for an electrochemical cell in the presence of both organic solubilised DMFc and predominantly interfacial Mo_2C at approximately pH 2 (Fig. 8(B)). The current of the irreversible wave (sampled at $\Delta_o^w\phi$ = 0.25 V for each scan rate) varied linearly with the square root of the scan rate indicating that the kinetics of the PCET process were controlled by linear diffusion, perhaps of DMFc to the catalytic reaction site at the interface or in the bulk 1,2-DCE.

4. Conclusions

Mo_2C and MoB have been identified as efficient catalysts for the reduction of aqueous protons to molecular hydrogen by organic electron donors such as decamethylferrocene. The activities exhibited by these inexpensive materials of exceptional abundance, due to their widespread use in industry, rival that of Pt microparticles of similar dimensions under biphasic conditions. This work highlights their suitability to act as HECs under acidic conditions, a key advantage due to the recognised limited availability of non-noble acid stable electrocatalysts for water splitting. The primary factors that influence catalytic activity are catalyst morphology and electrical conductivity. Thus, future perspectives involve the design of nano-sized Mo_2C or MoB and supporting these nano-catalysts on conductive carbon substrates such as carbon nanotubes, graphene or mesoporous carbon nanospheres. Further spectroscopic, electrochemical, and computational studies, as pioneered to elucidate the intricacies of catalytic hydrogen evolution at the surface of MoS_2 over the past decade, are warranted to answer fundamental questions regarding the specific mechanisms of hydrogen evolution at these transition metal carbide and boride surfaces.

Acknowledgements

This work was financially supported by the SNF grant ''Solar Fuels'' 200 021-134 745. The work in LSCI is supported by a starting grant from the European Research Council under the European Community's Seventh Framework Programme (FP7)/ERC Grant agreement no 257096. The authors wish to thank Pekka Peljo (Aalto University, Finland) for numerous useful discussions regarding the kinetic analysis.

References

1 J. O. M. Bockris, *Int. J. Hydrogen Energy*, 2002, **27**, 731–740.
2 G. W. Crabtree and M. S. Dresselhaus, *MRS Bull.*, 2008, **33**, 421–428.
3 A. Sartbaeva, V. L. Kuznetsov, S. A. Wells and P. P. Edwards, *Energy Environ. Sci.*, 2008, **1**, 79–85.
4 M. Pagliaro, A. G. Konstandopoulos, R. Ciriminna and G. Palmisano, *Energy Environ. Sci.*, 2010, **3**, 279–287.
5 Z. Samec, *Pure Appl. Chem.*, 2004, **76**, 2147–2180.
6 D. W. M. Arrigan, *Anal. Lett.*, 2008, **41**, 3233–3252.
7 P. Vanýsek and L. B. Ramírez, *J. Chil. Chem. Soc.*, 2008, **53**, 1455–1463.
8 H. H. Girault, in *Electroanalytical Chemistry, A Series of Advances*, ed. A. J. Bard and C. G. Zoski, CRC Press, Boca Raton, 2010, vol. 23, pp. 1–104.
9 Z. Samec, *Electrochim. Acta*, 2012, **84**, 21–28.
10 B. Su, R. Partovi-Nia, F. Li, M. Hojeij, M. Prudent, C. Corminboeuf, Z. Samec and H. H. Girault, *Angew. Chem., Int. Ed.*, 2008, **120**, 4753–4756.
11 I. Hatay, B. Su, F. Li, R. Partovi-Nia, H. Vrubel, X. Hu, M. Ersoz and H. H. Girault, *Angew. Chem., Int. Ed.*, 2009, **48**, 5139–5142.
12 M. A. Méndez, R. Partovi-Nia, I. Hatay, B. Su, P. Ge, A. Olaya, N. Younan, M. Hojeij and H. H. Girault, *Phys. Chem. Chem. Phys.*, 2010, **12**, 15163–15171.
13 B. Su, I. Hatay, P. Y. Ge, M. Méndez, C. Corminboeuf, Z. Samec, M. Ersoz and H. H. Girault, *Chem. Commun.*, 2010, **46**, 2918–2919.
14 B. Su, I. Hatay, F. Li, R. Partovi-Nia, M. A. Méndez, Z. Samec, M. Ersoz and H. H. Girault, *J. Electroanal. Chem.*, 2010, **639**, 102–108.
15 I. Hatay, B. Su, F. Li, M. A. Méndez, T. Khoury, C. P. Gros, J.-M. Barbe, M. Ersoz, Z. Samec and H. H. Girault, *J. Am. Chem. Soc.*, 2009, **131**, 13453–13459.
16 R. Partovi-Nia, B. Su, F. Li, C. P. Gros, J.-M. Barbe, Z. Samec and H. H. Girault, *Chem.–Eur. J.*, 2009, **15**, 2335–2340.
17 A. Trojánek, J. Langmaier, B. Su, H. H. Girault and Z. Samec, *Electrochem. Commun.*, 2009, **11**, 1940–1943.
18 I. Hatay, B. Su, M. A. Méndez, C. Corminboeuf, T. Khoury, C. P. Gros, M. Bourdillon, M. Meyer, J.-M. Barbe, M. Ersoz, S. Záliš, Z. Samec and H. H. Girault, *J. Am. Chem. Soc.*, 2010, **132**, 13733–13741.
19 B. Su, I. Hatay, A. Trojánek, Z. Samec, T. Khoury, C. P. Gros, J.-M. Barbe, A. Daina, P.-A. Carrupt and H. H. Girault, *J. Am. Chem. Soc.*, 2010, **132**, 2655–2662.
20 Y. Li, S. Wu and B. Su, *Chem.–Eur. J.*, 2012, **18**, 7372–7376.
21 A. J. Olaya, D. Schaming, P.-F. Brevet, H. Nagatani, T. Zimmermann, J. Vanicek, H.-J. Xu, C. P. Gros, J.-M. Barbe and H. H. Girault, *J. Am. Chem. Soc.*, 2012, **134**, 498–506.
22 P. Peljo, L. Murtomäki, T. Kallio, H.-J. Xu, M. Meyer, C. P. Gros, J.-M. Barbe, H. H. Girault, K. Laasonen and K. Kontturi, *J. Am. Chem. Soc.*, 2012, **134**, 5974–5984.
23 S. Wu and B. Su, *Chem.–Eur. J.*, 2012, **18**, 3169–3173.
24 U. Koelle, P. P. Infelta and M. Graetzel, *Inorg. Chem.*, 1988, **27**, 879–883.
25 P. Ge, M. D. Scanlon, A. J. Olaya, I. Hatay Patir and Hubert H. Girault, *ChemPhysChem*, submitted.
26 P. Ge, T. K. Todorova, I. H. Patir, A. J. Olaya, H. Vrubel, M. Mendez, X. Hu, C. Corminboeuf and H. H. Girault, *Proc. Natl. Acad. Sci. U. S. A.*, 2012, **109**, 11558–11563.
27 J. J. Nieminen, I. Hatay, P. Ge, M. A. Méndez, L. Murtomaki and H. H. Girault, *Chem. Commun.*, 2011, **47**, 5548–5550.

28 R. B. Gordon, M. Bertram and T. E. Graedel, *Proc. Natl. Acad. Sci. U. S. A.*, 2006, **103**, 1209–1214.
29 C.-J. Yang, *Energy Policy*, 2009, **37**, 1805–1808.
30 I. Hatay, P. Y. Ge, H. Vrubel, X. Hu and H. H. Girault, *Energy Environ. Sci.*, 2011, **4**, 4246–4251.
31 P. Ge, M. D. Scanlon, P. Peljo, X. Bian, H. Vubrel, A. O'Neill, J. N. Coleman, M. Cantoni, X. Hu, K. Kontturi, B. Liu and H. H. Girault, *Chem. Commun.*, 2012, **48**, 6484–6486.
32 H. Vrubel and X. Hu, *Angew. Chem., Int. Ed.*, 2012, **51**, 12703–12706.
33 S. Wirth, F. Harnisch, M. Weinmann and U. Schröder, *Appl. Catal., B*, 2012, **126**, 225–230.
34 D. V. Esposito, S. T. Hunt, Y. C. Kimmel and J. G. G. Chen, *J. Am. Chem. Soc.*, 2012, **134**, 3025–3033.
35 M. C. Weidman, D. V. Esposito, I. J. Hsu and J. G. Chen, *J. Electrochem. Soc.*, 2010, **157**, F179–F188.
36 M. C. Weidman, D. V. Esposito, Y.-C. Hsu and J. G. Chen, *J. Power Sources*, 2012, **202**, 11–17.
37 R. B. Levy and M. Boudart, *Science*, 1973, **181**, 547–549.
38 D. Ham and J. Lee, *Energies*, 2009, **2**, 873–899.
39 D. R. McIntyre, G. T. Burstein and A. Vossen, *J. Power Sources*, 2002, **107**, 67–73.
40 S. T. Oyama, *Catal. Today*, 1992, **15**, 179–200.
41 WebElements homepage. http://www.webelements.com (accessed November 2012).
42 Metal-Pages homepage. http://www.metal-pages.com (accessed November 2012).
43 Platinum Today homepage. http://www.platinum.matthey.com/pgm-prices/price-charts/(accessed November 2012).
44 J. G. Chen, *Chem. Rev.*, 1996, **96**, 1477–1498.
45 R. Koc and S. K. Kodambaka, *J. Eur. Ceram. Soc.*, 2000, **20**, 1859–1869.
46 F. Teng, J. Wang, X. An, B. Lu, Y. Su, C. Gong, P. Zhang, Z. Zhang and E. Xie, *RSC Adv.*, 2012, **2**, 7403–7405.
47 V. Domnich, S. Reynaud, R. A. Haber and M. Chhowalla, *J. Am. Ceram. Soc.*, 2011, **94**, 3605–3628.
48 R. Mitra, V. V. Rama Rao and A. Venugopal Rao, *Intermetallics*, 1999, **7**, 213–232.
49 A. Zahl, R. van Eldik, M. Matsumoto and T. W. Swaddle, *Inorg. Chem.*, 2003, **42**, 3718–3722.
50 D. J. Fermin, H. Dung Duong, Z. Ding, P.-F. Brevet and H. H. Girault, *Phys. Chem. Chem. Phys.*, 1999, **1**, 1461–1467.
51 M. Von Smoluchowski, in *Handbuch der Electrizität und des Magnetismus (Graetz)*, Barth, Leipzig, 1921, vol. 2, p. 366.
52 A. V. Delgado, F. González-Caballero, R. J. Hunter, L. K. Koopal and J. Lyklema, *Pure Appl. Chem.*, 2005, **77**, 1753–1805.
53 D. C. Henry, *Proc. R. Soc. London*, 1931, **A133**, 106–129.
54 W. H. Binder, *Angew. Chem., Int. Ed.*, 2005, **44**, 5172–5175.
55 M. M. Gudarzi and F. Sharif, *Soft Matter*, 2011, **7**, 3432–3440.
56 T. Wandlowski, V. Mareček and Z. Samec, *Electrochim. Acta*, 1990, **35**, 1173–1175.
57 D. Gosset and M. Colin, *J. Nucl. Mater.*, 1991, **183**, 161–173.
58 C.-H. Jung, M.-J. Lee and C.-J. Kim, *Mater. Lett.*, 2004, **58**, 609–614.
59 K. J. Leary, J. N. Michaels and A. M. Stacy, *J. Catal.*, 1986, **101**, 301–313.
60 K. J. Leary, J. N. Michaels and A. M. Stacy, *J. Catal.*, 1987, **107**, 393–406.
61 K. Oshikawa, M. Nagai and S. Omi, *J. Phys. Chem. B*, 2001, **105**, 9124–9131.
62 K. M. Andersson and L. Bergström, *Int. J. Refract. Met. Hard Mater.*, 2000, **18**, 121–129.
63 F. Harnisch, U. Schröder, M. Quaas and F. Scholz, *Appl. Catal., B*, 2009, **87**, 63–69.
64 P. D. Williams and D. D. Hawn, *J. Am. Ceram. Soc.*, 1991, **74**, 1614–1618.
65 M. Sandlin, D. Butt, T. Taylor and J. Petrovic, *J. Mater. Sci. Lett.*, 1997, **16**, 1336–1338.
66 V. J. Cunnane, D. J. Schiffrin, C. Beltran, G. Geblewicz and T. Solomon, *J. Electroanal. Chem. Interfacial Electrochem.*, 1988, **247**, 203–214.
67 T. Kakiuchi, in *Liquid–liquid interfaces, Theory and Methods*, ed. A. G. Volkov and D. W. Deamer, CRC Press, Boca Raton, 1996, pp. 1–18.
68 P. W. Atkins, *Physical Chemistry*, Oxford University Press, Oxford, 1990.
69 V. Stamenkovic, B. S. Mun, K. J. J. Mayrhofer, P. N. Ross, N. M. Markovic, J. Rossmeisl, J. Greeley and J. K. Nørskov, *Angew. Chem., Int. Ed.*, 2006, **45**, 2897–2901.
70 J. K. Nørskov, T. Bligaard, A. Logadottir, J. R. Kitchin, J. G. Chen, S. Pandelov and U. Stimming, *J. Electrochem. Soc.*, 2005, **152**, J23–J26.
71 B. Hinnemann, P. G. Moses, J. Bonde, K. P. Jørgensen, J. H. Nielsen, S. Horch, I. Chorkendorff and J. K. Nørskov, *J. Am. Chem. Soc.*, 2005, **127**, 5308–5309.
72 J. K. Nørskov, T. Bligaard, J. Rossmeisl and C. H. Christensen, *Nat. Chem.*, 2009, **1**, 37–46.